Analysis of Side-Chain Organization on a Refined Model of Charybdotoxin: Structural and Functional Implications[†]

François Bontems, Bernard Gilquin, Christian Roumestand, André Ménez, and Flavio Toma*

Département d'Ingénierie et d'Etude des Protéines, Laboratoire de Structure des Protéines en Solution, CE-Saclay, 91191 Gif-sur-Yvette Cedex, France

Received March 16, 1992; Revised Manuscript Received May 14, 1992

ABSTRACT: The spatial organization of side chains on a refined model of charybdotoxin is presented. First, the structural role of two groups of well-defined, low-accessible side chains (Thr_3, Val_5, Val_{16}, Leu_{20}, Cys_{33} and Leu_{20}, His_{21}, Thr_{23}, Cys_{17}, Cys_{35}) is discussed. These side chains are conserved in three out of the five known scorpion toxins acting on K^+ channels. Interestingly, they are not conserved in scyllatoxin which presents a slightly different secondary structure organization. Second, the spatial organization of all positively charged residues is analyzed. Comparison with the results presented by Park and Miller [(1992) *Biochemistry* (preceding paper in this issue)] shows that all functionally important positive residues are located on the β-sheet side of the toxin. These results are different from those obtained by Auguste et al. [(1992) *Biochemistry 31*, 648–654] on scyllatoxin, which blocks a different type of K^+ channel. This study shows, in fact, that functionally important positive residues are located on the helix side of the toxin. Thus, charybdotoxin and scyllatoxin, which present the same global fold, interact with two different classes of K^+ channels by two different parts of the motif.

Venomous animals produce a variety of toxins that act on different types of channels. These toxins perturb the nervous and/or muscular system, providing an efficient means to subdue preys. Some of these toxins have been extensively studied with respect to their structure, mode of action, and localization of the functional site. These are the toxins acting on acetylcholine receptor, in particular α-conotoxins (Olivera et al., 1990) and snake toxins (Endo & Tamiya, 1991), toxins acting on Na^+ channels like sea anemone (Norton, 1991) and scorpion toxins (Simard & Watt, 1990), and toxins acting on K^+ channels such as honeybee toxins (Dreyer, 1990). More recently, a new family of toxins isolated from the venom of scorpions and acting on K^+ channels has been characterized (Dreyer, 1990; Strong, 1990). These toxins seem to act on different types of K^+ channels, even though they have related sequences with 30–40 amino acids and three disulfide bridges. Very little is known about the structural basis for the expression of the K^+ blocking activity of these molecules. We have recently reported the global three-dimensional structure of one of these toxins, called charybdotoxin (Chtx)[1] (Bontems et al., 1991a). However, the precision of the structure was not sufficient to describe the fine detail of the molecule and, in particular, the spatial organization of the side chains. In this paper, we report the refined structure of charybdotoxin and discuss the organization of the side chains within the molecule. Some of them seem to be important in the conservation of the structure whereas others may have a functional role. Furthermore, the structure we describe here provides precise molecular support for the results reported by Park and Miller (1992) on the site-directed mutagenesis of Chtx.

MATERIALS AND METHODS

Biological Sample. As previously described, all experiments were carried out using 8 mg of pure, natural charybdotoxin isolated from 2.5 g of scorpion venom (Bontems et al., 1991a): 7 mg was dissolved in 400 μL of 90% H_2O and 10% D_2O (final concentration: 4 $mmol{\cdot}L^{-1}$) and 1 mg was dissolved in 400 μL of D_2O (final concentration: 0.6 $mmol{\cdot}L^{-1}$). The pH of both samples was adjusted to 3.5, using microliter amounts of HCl or DCl. Purity and activity of the toxin were checked before and after completion of the study in order to verify that no degradation had occurred during the experiments.

NMR Spectroscopy. All proton NMR spectra were recorded at 600 MHz with a Bruker AM600 or AMX600 spectrometer equipped with a H_2O suppression selective probe.

The identification of NOEs was achieved using TOCSY (Davis & Bax, 1985), COSY (Aue et al., 1976), and NOESY (Kumar et al., 1980) experiments, recorded either in H_2O or in D_2O at temperatures ranging between 15 and 45 °C. The quality of similar spectra has been illustrated previously, and the complete resonance assignment has already been reported (Bontems et al., 1991a). TOCSYs were recorded with an isotropic mixing time of 80 ms and NOESYs with mixing times of 100, 150, and 300 ms in order to identify spin diffusion effects. A 5% random variation in NOESY mixing times was used in order to avoid zero-quantum coherences (Macura et al., 1981). Acquisition consisted in 512 fids of 96 scans, each scan being 2048 time-domain data points.

$^3J_{HN-H\alpha}$ and $^3J_{H\alpha-H\beta}$ were measured using DQF-COSY (Rance et al., 1983) at 45 °C in H_2O and D_2O, respectively. Typical experiments were recorded with 1024 fids of 128 scans, each scan being 4096 time-domain data points.

NOE buildup was followed using NOESY experiments recorded in H_2O at 45 °C with eight mixing times ranging from 50 to 300 ms. Each experiment consisted in 512 fids of 96 scans, each scan being 2048 time-domain data points.

Amide proton–deuterium exchange data were obtained at 15 °C from a series of absolute value COSY experiments consisting of 256 fids of 4 scans, each scan being 1024 time-

---

[†] The coordinates of the set of structures of charybdotoxin presented in this work will be deposited in the Brookhaven Protein Data Bank.

* To whom correspondence should be addressed.

[1] Abbreviations: Chtx, charybdotoxin; Chtx-2, charybdotoxin-2; NMR, nuclear magnetic resonance; noe, nuclear Overhauser effect; TOCSY, total correlation spectroscopy; COSY, correlation spectroscopy; NOESY, nuclear Overhauser effect spectroscopy; DQF-COSY, double-quantum-filtered correlation spectroscopy; Z, one-letter code for pyroglutamic acid.

0006-2960/92/0431-7756$03.00/0

Table I: Different Steps of the Refinement Protocol Presented Together with the Evolution of the Parameters: Temperature, Force Field Constants, and Experimental Restraint Constants[a]

	evolution of parameters			
DIANA structures				
minimization	K_{bond}	400		
10 cycles with descendant harmonic constraints (1000–100)	K_{angle}	40		
10 cycles with descendant harmonic constraints (100–10)	K_{dihe}	5	K_{vdw}	10
10 cycles with descendant harmonic constraints (10–1)	$K_{S\text{–}S}$	0		
minimization without constraints	$K_{C\text{–}S\text{–}S}$	0	K_{noe}	0
	$K_{C\text{–}S\text{–}S\text{–}C}$	0	K_{cdihe}	0
minimized structures	K_{bond}	400	temp	0 K
	K_{angle}	40		
	K_{dihe}	0	K_{vdw}	0.002
	$K_{S\text{–}S}$	0.1		
	$K_{C\text{–}S\text{–}S}$	0.1	K_{noe}	0.1
	$K_{C\text{–}S\text{–}S\text{–}C}$	0.1	K_{cdihe}	0.1
thermalization	K_{bond}	500	temp	1000 K
20 cycles of 200 steps of dynamics	K_{angle}	500		
parameters and temperature incremented every cycle	K_{dihe}	0	K_{vdw}	0.002
	$K_{S\text{–}S}$	500		
	$K_{C\text{–}S\text{–}S}$	500	K_{noe}	50
	$K_{C\text{–}S\text{–}S\text{–}C}$	3	K_{cdihe}	20
first equilibration	K_{bond}	500	temp	1000 K
8000 steps of dynamics	K_{angle}	500		
with the current parameters	K_{dihe}	0	K_{vdw}	4
increment of the repulsive potential	$K_{S\text{–}S}$	500		
10 cycles of 200 steps of dynamics	$K_{C\text{–}S\text{–}S}$	500	K_{noe}	50
vdw constant incremented every cycle	$K_{C\text{–}S\text{–}S\text{–}C}$	3	K_{cdihe}	20
second equilibration	K_{bond}	400	temp	0 K
8000 steps of dynamics	K_{angle}	40		
with the current parameters	K_{dihe}	0	K_{vdw}	4
cooling	$K_{S\text{–}S}$	400		
80 cycles of 500 steps of dynamics	$K_{C\text{–}S\text{–}S}$	40	K_{noe}	50
force field constants and temperature gradually decreased	$K_{C\text{–}S\text{–}S\text{–}C}$	3	K_{cdihe}	20
annealed structure				
final minimization	parmallh3x	parameters	temp	0 K
500 steps of dynamics			K_{noe}	50
utilization of the standard X-PLOR energy function			K_{cdihe}	20
final structures				

[a] K_{bond}, K_{angle}, and K_{dihe} are the force constants of bond, angle, and dihedral potentials used for all residues except cystines. $K_{S\text{–}S}$, $K_{C\text{–}S\text{–}S}$, and $K_{C\text{–}S\text{–}S\text{–}C}$ indicate the values used for the cystine S^γ–S^γ bonds, C^β–S^γ–S^γ angles, and χ_2 and χ_3 dihedral angles (C^α–C^β–S^γ–S^γ and C^β–S^γ–S^γ–C^β). K_{vdw} is the force constant of the repulsive potential: $E_{vdw} = K_{vdw}(R^2 - R_0{}^2)^2$ (R is the distance between two nuclei; R_0 is the sum of the two van der Waals radii). K_{noe} and K_{dihe} are the two experimental restraint force constants.

domain data points. The relaxation delay was shortened to 0.70 s, so that one experiment could be completed in less than 15 min.

All phase-sensitive spectra were acquired using the time-proportional phase incrementation method (Redfield & Kuntz, 1975). The simultaneous or sequential acquisition mode was used depending on the spectrometer (AMX600 or AM600, respectively). In the second case, the baseline of the ω_2 slices was optimized by adjusting the receiver reference phase and the delay between the last pulse and the acquisition of the first data point in order to obtain a spectrum which needed no zero- or first-order phase correction after Fourier transform. All experiments were zero filled in f_1 in order to achieve the same resolution in each dimension. They were multiplied by a shifted sine-bell in both dimensions prior to Fourier transform. Data processing was carried out with the programs UXNMR or NMRI on a Bruker X32 or Sun Sparc station 1, respectively.

Experimental Restraints. Analysis of the NOESY spectra led to the identification of 144 interresidue NOEs corresponding to 72 sequential, 20 nonsequential backbone/backbone, 19 nonsequential side-chain/backbone, and 33 nonsequential side-chain/side-chain connectivities. The intensities of the sequential and nonsequential backbone/backbone connectivities were estimated either from the measurement of the buildup rates or from the measurement of the cross-peak volumes in spectra recorded with a 150-ms mixing time. They were classified into three groups, i.e., small, medium, and large. The corresponding distance restraints were calibrated by comparison with known distances in regular secondary structures (2.2 Å for $d_{\alpha N}$ in a β-sheet, 2.8 Å for d_{NN} in an helix); upper bounds were set to 2.5, 3.0, or 4.0 Å for large, medium, or small effects, respectively. All other distances were set to 4.0 Å. In addition, seven intraresidue restraints were used.

Measurement of the amide proton/deuterium exchange kinetics allowed the identification of 11 hydrogen bonds (6 in the sheet and 5 in the helix), leading to the introduction of 22 restraints ($d_{HN\text{–}O} = 2.2$ Å, $d_{N\text{–}O} = 3.2$ Å) in the calculations.

Thirty φ angles were deduced from the values of ${}^3J_{HN\text{–}H\alpha}$ coupling constants distributed as follows: 21 in the sheet and in the 1–9 region were constrained using $\varphi = -120 \pm 25°$ (${}^3J_{H\alpha} > 9$ Hz) to $\varphi = -120 \pm 55°$ (${}^3J_{H\alpha} = 8$ Hz); 7 in the helix were constrained using $\varphi = -60 \pm 25°$ (${}^3J_{H\alpha} = 4$ Hz) to $\varphi = -80 \pm 25°$ (${}^3J_{H\alpha} = 7$ Hz); the two φ_{30} and φ_{31} angles of the type I β-turn were set to $-80 \pm 25°$ (${}^3J_{H\alpha} = 7$ Hz).

Measurement of ${}^3J_{H\alpha\text{–}H\beta}$ and identification of HN–H^β, HN–$H^{\beta'}$, H^α–H^β, and H^α–$H^{\beta'}$ intraresidue NOEs led to the determination of χ_1 angles for 12 residues including the 6 half-cystines. These angles have been restrained to $-60 \pm 45°$, $180 \pm 45°$, or $60 \pm 45°$ according to the rotamer found.

Structure Computations. Structures of charybdotoxin have been computed using a procedure combining minimization in the dihedral space with the program DIANA (Günter et al.,

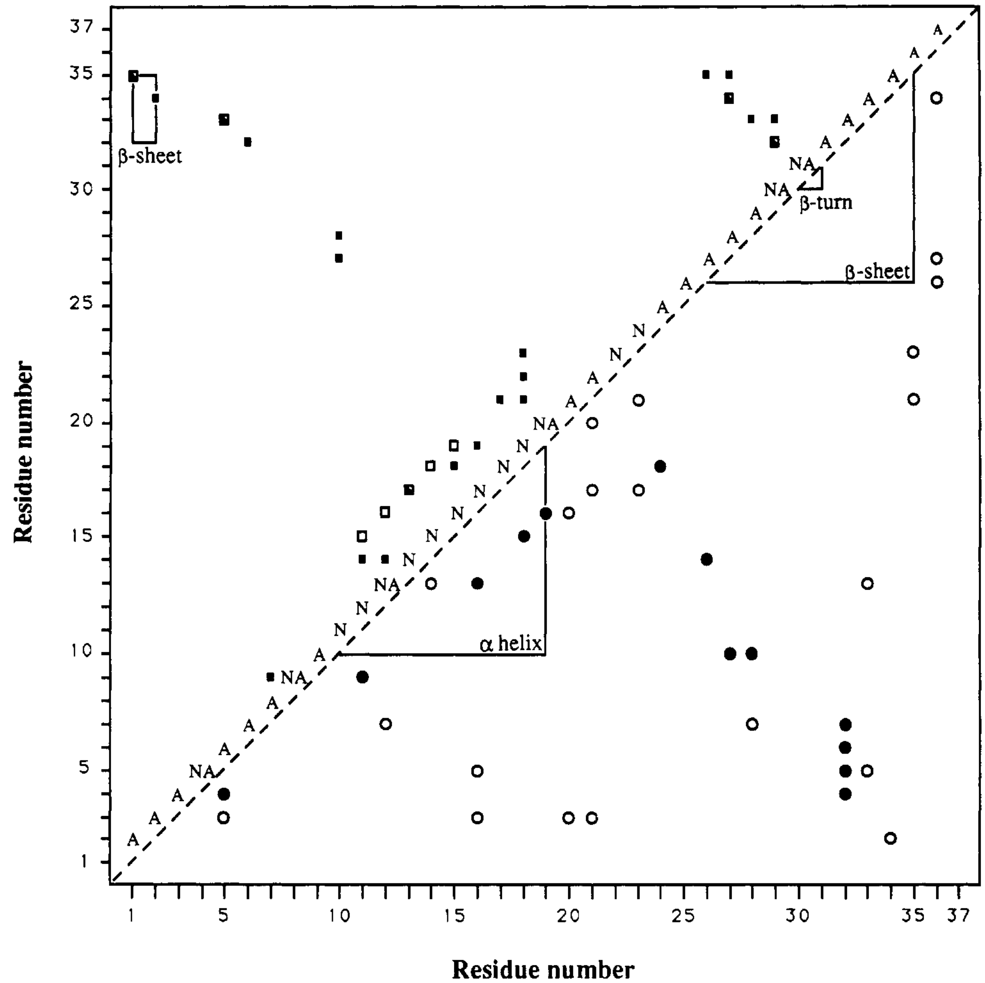

FIGURE 1: Diagonal plot of distance restraints. On the diagonal, A and N indicate H^{α}–HN and HN–HN sequential effects, respectively. The remaining sequential effects have been omitted for clarity. Off-diagonal points indicate one (or more) effect(s) between residues at positions shown along the axis. Above the diagonal: (■) backbone/backbone NOEs; (□) hydrogen bonds; (▣) NOEs and hydrogen bonds. Below the diagonal: (●) backbone/side-chain NOEs; (○) side-chain/side-chain NOEs.

1991) and simulated annealing (Brünger et al., 1987) with the program X-PLOR (Brünger, 1988). The approach proved to be particularly fruitful. DIANA allowed the fast generation of a great number of conformations which were useful to refine the set of restraints. These structures have a high internal energy. They were, thus, further refined by simulated annealing using X-PLOR.

Once the complete set of experimental restraints was established, 25 structures were generated with DIANA, using a standard protocol. At this step, 15 additional restraints were introduced in order to maintain the disulfide bridges as close as possible to their standard geometry [S^{γ_i}–S^{γ_j} = 2.1 Å, S^{γ_i}–C^{β_j} and C^{β_i}–S^{γ_j} = 3.5 Å, C^{β_i}–C^{β_j} = 4.5 Å, and C^{α_i}–C^{α_j} = 6.5 Å (Srinivasan et al., 1990) for each bridge].

The 12 best DIANA structures were refined by simulated annealing. The resulting structures both satisfy the experimental restraints and have low total energy values. Our protocol was derived from the one described by Gippert et al. (1990). We used the same energy function as Nilges et al. (1988). It contained no electrostatic potential, and a simple repulsive term was used instead of the van der Waals potential. This function accelerates the calculations and allows a better exploration of the conformational space. High-temperature dynamics was performed using increasing values of the geometrical force constants. However, this force field is not adapted at low temperature. Thus, the force field was gradually modified during the heating and the cooling steps of the protocol. The temperature was controlled during the process by coupling the system to a thermal bath, by using a friction coefficient in the Langevin dynamic algorithm with zero random force (Brünger et al., 1991). The time step was set to 0.5 fs.

The main steps of the refinement protocol are summarized in Table I.

In the first step, the structures were minimized in order to remove all the strains. No experimental constraints were introduced in this step. The force field constants were adapted from those used at 300 K except for the disulfides. The disulfide geometry was, in fact, very poor in the DIANA structures, so the corresponding force constants were set to zero. A harmonic potential was imposed on all atoms in order to prevent large shifts in the first steps of the minimization. This potential was gradually removed, allowing complete minimization.

In the second step (thermalization and first equilibration), the temperature, force field constants, and experimental restraint constants were gradually increased. This was followed by an equilibration allowing the system to explore the conformational space. A small value of the repulsive force constant was used in order to promote rearrangements in the structure.

In the third step (van der Waals and second equilibration), the repulsive potential force constant was increased.

In the fourth step (cooling), the temperature and the force field constants were slowly decreased in order to drive the system toward the deepest minima.

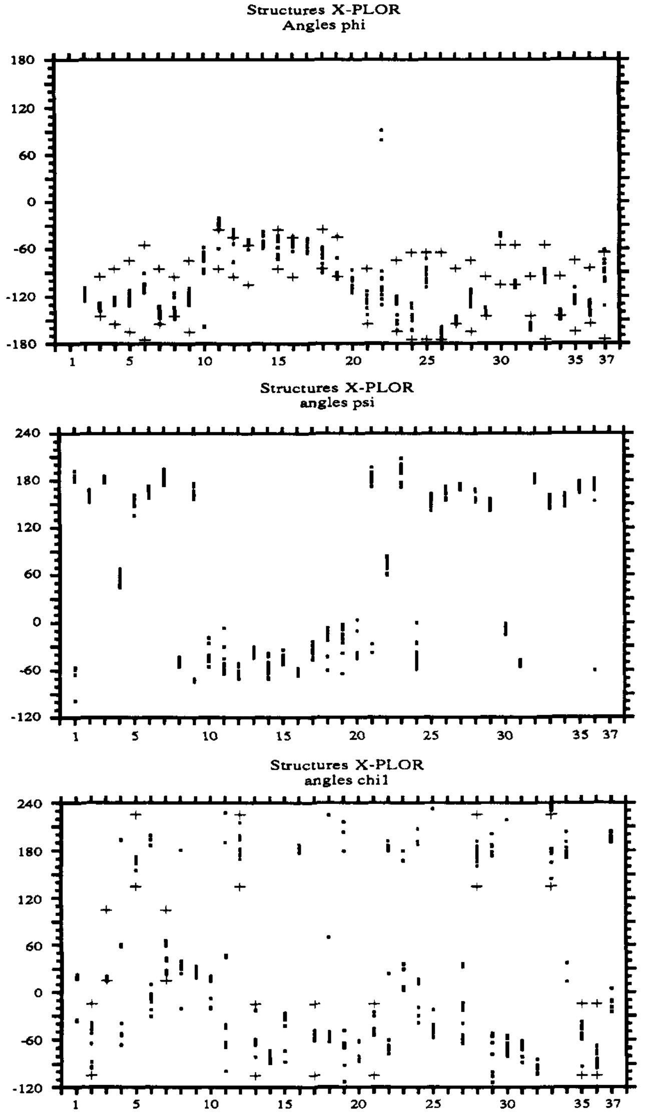

FIGURE 2: Values of the φ (top), ψ (middle), and χ_1 (bottom) angles calculated for each structure (|) presented together with the φ and χ_1 angle restraints used for the calculation (X-PLOR). The upper and lower bounds are indicated by a (+).

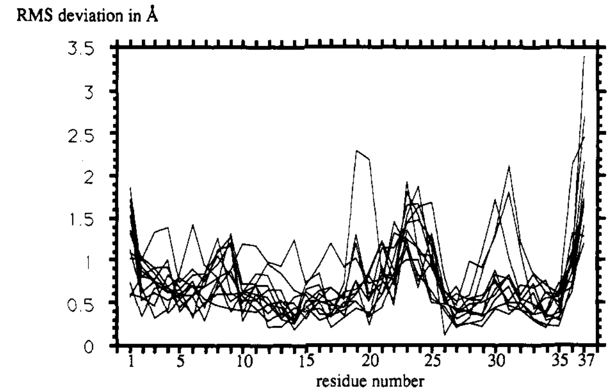

FIGURE 3: ⟨rmsd⟩ calculated on the backbone atoms as a function of the residue number between each DIANA structure and the average structure.

Finally, a short dynamics was performed with all restraints, using a final temperature setting of 0 K. The standard X-PLOR energy function (with electrostatic and van der Waals terms) and the parmallh3x.pro parameter file were used. This allows a final optimization of the structure and gives a value for the total energy comparable to those of the literature.

Analysis of the Structures. The structural features were calculated using X-PLOR. This analysis was completed by visual inspection of the molecules, using SYBYL on an E&S PS390 graphic station.

RESULTS

NMR experiments provided a set of distance and dihedral angle restraints from which different structures of Chtx were derived by the computational procedure described under Materials and Methods. The interresidue distance restraints deduced from the NOE measurements are summarized in Figure 1. The φ and χ_1 angle restraints deduced from the vicinal coupling constants are illustrated in Figure 2. This figure will be further discussed in the following paragraphs.

DIANA *Structures.* Twenty-five starting conformations were obtained with DIANA. Among these, 12 structures present no distance violations greater than 1 Å and have a target function value smaller than 10. All distance violations are randomly distributed; most of them are smaller than 0.5 Å and correspond to backbone/backbone and backbone/side-chain distances. Two dihedral angles (φ_{30} and φ_{31}) are systematically violated even though the violations remain small (<30°). The other dihedral angle restraints are satisfied. In particular, it is worth noting that no violation occurs on half-cystine χ^1 angles.

These structures are well-defined, as shown by the value of the average root mean square deviation (⟨rmsd⟩) as calculated on the backbone between all pairs of structures (1.25 Å) or between all structures and the average structure (0.85 Å). The backbone deviation between each structure and the average structure calculated for each residue (Figure 3) shows that the largest structural variations occur at the N- and C-terminal residues (Pgl$_1$, Tyr$_{36}$, and Ser$_{37}$) and in the Thr$_{21}$–Arg$_{25}$ region. A few structures present larger deviations of the backbone from the average structure and are located at positions 8–9, 29–32, and 19–20.

X-PLOR *Structures.* The 12 best DIANA structures were refined by simulated annealing with X-PLOR, yielding 12 low-energy structures. These structures satisfy both the experimental restraints and the covalent geometry parameters (Table II). They present 0–2 distance violations ranging from 0.1 to 0.13 Å and 2–5 angle violations ranging from 5° to 20° (Figure 2). In five structures, however, the χ_1 angle of Cys$_{33}$ is close to −120° (eclipsed rotamer). Deviations from the ideal covalent structure are very small, as indicated by the low ⟨rmsd⟩ values for the bond lengths (0.013 Å) and for the angles (3.35°). The total energy (E_{total}) and the van der Waals energy (E_{vdw}), calculated with a standard energy function and the parmallh3x parameter file, are large and negative ($E_{\text{total}} < -1200$ kcal·mol^{-1}; $E_{\text{vdw}} < -120$ kcal·mol^{-1}), indicating, in particular, that there are no bad nonbonded contacts.

Description of the Backbone. Altogether, these results converge toward very close backbone structures for the 12 computed structures as shown by the small ⟨rmsd⟩ values (0.64 Å as calculated between all pairs of structures and 0.44 Å between all structures and the average structure). This is illustrated in greater detail by the absence of dispersion of the computed values of the φ and ψ angles for most residues (Figure 2). The backbone superposition of eight such structures is presented in Figure 4. Charybdotoxin contains a small three-stranded antiparallel β-sheet (strand I, residues 1–2; strand II, residues 25–29; strand III, residues 32–36). This is linked to an α-helix (residues 10–19) by two disulfides (Cys$_{13}$–Cys$_{33}$, Cys$_{17}$–Cys$_{35}$) and to an extended fragment (residues 4–7) by the third disulfide (Cys$_7$–Cys$_{28}$). The axis of the helix forms an approximate 45° angle with the axis of the sheet, while the extended 4–7 fragment is almost perpendicular to the latter

Table II: Overview of the Energy and Geometry Features of X-PLOR Structures[a]

	energy									violations				rms		
	E_{total}	E_{bond}	E_{angle}	E_{dihe}	E_{impr}	E_{vdw}	E_{elec}	E_{noe}	E_{cdihe}	bond	angle	noe	cdihe	bond	angle	noe
A, X-PLOR	−1357	18	168	184	6	−139	−1605	2.18	8.73	5	6	0	4	0.013	3.315	0.016
B, X-PLOR	−1308	19	172	166	5	−136	−1542	2.23	4.87	4	11	1	4	0.013	3.361	0.016
C, X-PLOR	−1323	19	165	175	5	−131	−1564	2.21	4.7	5	9	1	3	0.013	3.278	0.016
D, X-PLOR	−1271	19	172	182	5	−130	−1527	1.92	6.28	4	9	1	5	0.013	3.344	0.015
E, X-PLOR	−1320	19	167	168	5	−136	−1550	2.28	4.11	4	9	2	4	0.013	3.306	0.016
F, X-PLOR	−1296	19	175	170	6	−136	−1538	2.87	5.06	6	12	1	4	0.013	3.371	0.018
G, X-PLOR	−1284	20	173	178	6	−127	−1541	2.26	3.1	7	11	2	3	0.013	3.349	0.019
H, X-PLOR	−1253	18	167	173	4	−133	−1490	2.04	4.81	3	6	1	3	0.013	3.289	0.015
I, X-PLOR	−1329	19	174	158	5	−135	−1558	1.85	4.77	5	13	1	4	0.013	3.379	0.015
J, X-PLOR	−1347	19	166	169	5	−134	−1581	2.13	6.29	6	7	1	4	0.013	3.291	0.016
K, X-PLOR	−1344	17	162	172	5	−141	−1568	1.99	6.77	6	6	1	3	0.013	3.236	0.015
L, X-PLOR	−1283	18	163	182	5	−133	−1527	1.81	6.44	4	7	0	2	0.013	3.268	0.014

[a] The parameters characterizing the structures have been calculated with X-PLOR, using the standard energy function and the parmallh3x parameter file. E_{noe} and E_{dihe} have been calculated with $K_{noe} = 50$ kcal·mol^{-1}·Å^{-1} and $K_{dihe} = 20$ kcal·mol^{-1}·rd^{-2}. The number of reported violations corresponds to violations larger than 0.01 Å for bonds, 10° for angles, 0.1 Å for noe restraints, and 5° for dihedral restraints.

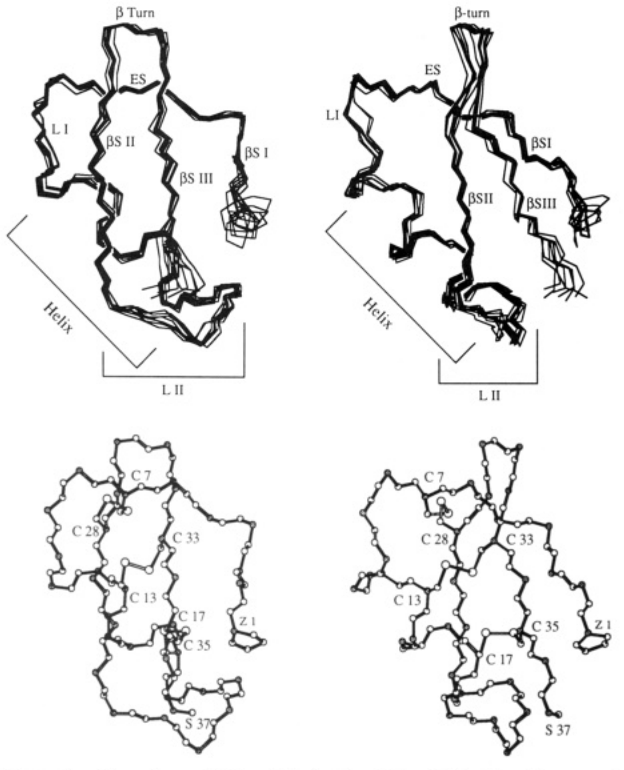

FIGURE 4: Structure of charybdotoxin. (Top) The backbones of eight charybdotoxin structures are superimposed. The disulfide bridges have been omitted for clarity. The different elements of the molecule are indicated: βSI, βSII, and βSIII are the three strands of the β-sheet; ES is the extended fragment; LI and LII are the two short loops connecting the helix to the extended fragment and the β-sheet, respectively. (Bottom) The disulfide bridges, in one structure, have been represented. The C$^{\alpha}$ atoms are in grey. Z is the one-letter code for pyroglutamic acid.

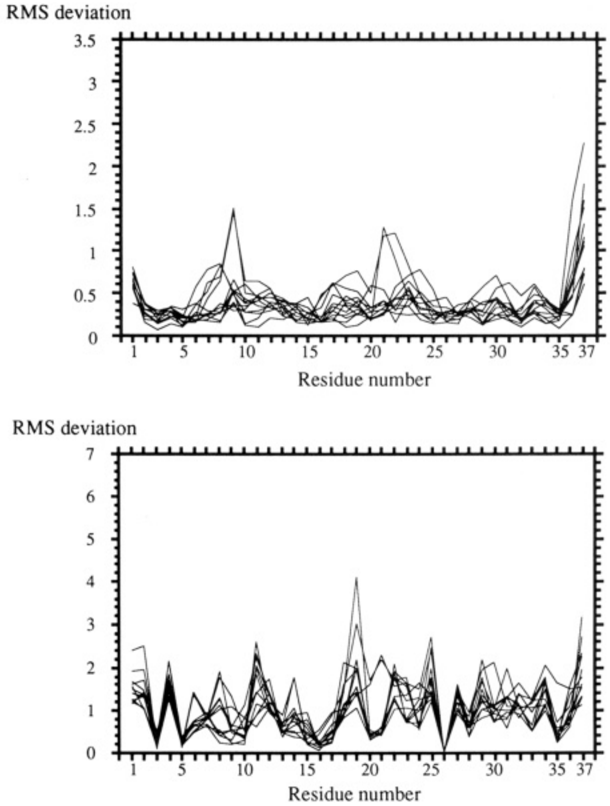

FIGURE 5: ⟨rmsd⟩ of the backbone (top) and side chains (bottom) calculated as a function of the residue number between each X-PLOR structure and the average structure.

axis. These structural elements are connected by two short loops (loop I, residues 8–9 between the fragment and the helix; loop II, residues 20–24 between the helix and β-strand II, residues 25–29) and by a type I β-turn (residues 30–31 between the second and the third strand of the sheet).

The deviation from the average backbone conformation was computed residue by residue in the 12 structures (Figure 5, top). The small ⟨rmsd⟩ values in all these indicate the excellent definition of the helix, the sheet, and the turn. The backbone structure appears less defined at both termini (Pgl$_1$, Tyr$_{36}$, Ser$_{37}$) and at Thr$_9$ as reflected by variations of ψ_1, ψ_{36}, and ψ_9 values (Figure 2). The His$_{21}$-Asn$_{22}$ region adopts an alternative conformation in two structures corresponding to different values of ψ_{21} and φ_{22} (Figure 2). In contrast to the backbone, the conformation of the disulfide bridges appears to be less defined. The disulfides were in fact found to fit two different conformations corresponding to opposite χ_3 values (i.e., ca. −100° and +100°/120°). In the case of Cys$_{13}$–Cys$_{33}$, the negative χ_3 value is found associated to an eclipsed rotamer for Cys$_{33}$. This conformation is thus unlikely. However, it must be noted that the conformational differences of the disulfides have a negligible influence on the backbone structure.

Description of the Side Chains. All side chains were further analyzed in two ways.

First, the ⟨rmsd⟩ from the average structure was calculated for each residue in the 12 structures (Figure 5, bottom), providing a picture of the spatial definition of the side chains. Second, the surface accessibility was calculated by comparing the solvent-accessible surface areas of a given side chain in

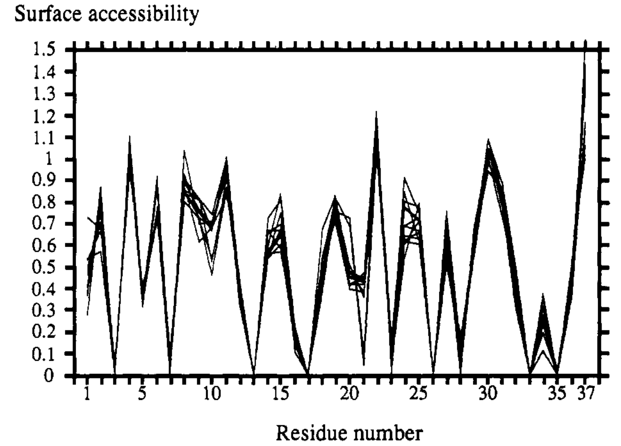

FIGURE 6: Side-chain surface accessibility of all X-PLOR structures calculated as a function of the residue number. The accessibility was calculated by comparing the surface accessible (radius probe 1.6 Å) of each residue in the structure and in the extended Gly-X-Gly peptide (Miller et al., 1987).

the protein and in the Gly-X-Gly peptide in the extended conformation (Miller et al., 1987) (Figure 6).

As shown by Figures 2 (χ_1 angle distributions) and 5, the side chains may have very different definitions. The side chains of Pgl$_1$, Phe$_2$, Asn$_4$, Lys$_{11}$, Arg$_{19}$, Arg$_{25}$, Met$_{29}$, and Ser$_{37}$ exhibit high atomic ⟨rmsd⟩, whereas the side chains of Thr$_3$, Val$_5$, Val$_{16}$, Leu$_{20}$, His$_{21}$, Cys$_{28}$, and Cys$_{35}$ exhibit on the opposite low ⟨rmsd⟩ values and have therefore a high spatial definition. Interestingly, analysis of $^3J_{\mathrm{H}\alpha-\mathrm{H}\beta}$ coupling constants and intraresidue NOEs indicates that the three χ_1 conformers of Asn$_4$ and Met$_{29}$ are equally populated, whereas a preferred side-chain rotamer was found for Thr$_3$, Val$_5$, Leu$_{20}$, His$_{21}$, Cys$_{28}$, and Cys$_{35}$ (Figure 2). Furthermore, most of the side-chain/side-chain NOEs observed in Chtx involve these latter residues. We observe, however, that three of these side chains (Leu$_{20}$, His$_{21}$, and Cys$_{35}$) may adopt two different conformations.

A similar result is found when the surface accessibility is analyzed. As shown by Figure 6, the accessibility of a given side chain is very similar in the 12 structures but may be very different for residues in the same structure. The surface accessibility is very large (>0.8) for seven residues and very low (<0.2) for ten residues. Most of the remaining residues have an intermediate solvent accessibility (0.5–0.8). The seven residues displaying high accessibility are Asn$_4$, Thr$_8$, Lys$_{11}$, Asn$_{22}$, Lys$_{31}$, Lys$_{32}$, and Ser$_{37}$. The ten residues exhibiting low accessibility are the six half-cystines, Thr$_3$, Val$_{16}$, Thr$_{23}$, and Gly$_{26}$.

These results are related to the observed side-chain/side-chain NOEs. Analysis of NOE experiments yielded 33 side-chain/side-chain effects (Figure 1). Twenty-six NOEs are found between a small number of residues organized into three groups. The first of these groups is formed by the side chains of residues Thr$_3$, Val$_5$, Val$_{16}$, Leu$_{20}$, and Cys$_{33}$, the second by the side chains of residues Cys$_{17}$, Leu$_{20}$, His$_{21}$, Thr$_{23}$, and Cys$_{35}$, and the third by the side chains of residues Phe$_2$, Lys$_{27}$, Arg$_{34}$, and Tyr$_{36}$. We notice that the first two groups are mostly composed of hydrophobic, well-defined, and low-accessible side chains.

DISCUSSION

The charybdotoxin molecule is made of a small structural motif composed of a short triple-stranded β-sheet, an α-helix, and an extended fragment linked together by three disulfide bridges. In a previous study, we compared the structure of charybdotoxin with those of two functionally unrelated long-chain scorpion toxins (Fontecilla-Camps et al., 1980, 1988) and showed that this motif forms the structural core of all known scorpion toxins and insect defensins (Bontems et al., 1991b). We discussed in particular the role of the conserved residues (six Cys and 1 Gly) forming a consensus sequence associated to the motif. In the present paper, we focus on the structural and possible functional role of the remaining side chains in charybdotoxin. Since charybdotoxin is a member of the family of scorpion toxins acting on K$^+$ channels, we compare its characteristics with those of the other toxins and in particular with those of scyllatoxin (leiurotoxin I). The preliminary structure (Martins et al., 1990) and the active site determination (Auguste et al., 1992) of scyllatoxin were reported. This comparison is based on our previous conclusion that the spatial organization of the backbone of the motif is conserved in all scorpion toxins (Bontems et al., 1991a,b). Moreover, comparison of the preliminary reported structure of scyllatoxin and of charybdotoxin shows that the secondary structure elements of these two molecules are located identically relative to the position of the Cys residues (Table III). It is thus likely that side chains of the motif at homologous sequential positions in these toxins have a similar organization in space. It is worth noting that this assumption may be valid for residues of the motif but not for residues of the loops connecting the different parts of the motif, as the loops may have various lengths, structures, and space orientations.

As shown under Results, most of the side chains of charybdotoxin present large ⟨rmsd⟩ and solvent accessibility values. Two groups of side chains, however, share many nonbonded contacts and have well-defined positions (Figure 7). One of them comprises residues from β-strand I (Thr$_3$), the extended fragment (Val$_5$), the helix (Val$_{16}$ and Leu$_{20}$), and β-strand III (C$^\beta$H$_2$ of Cys$_{33}$). These residues form a hydrophobic cluster. They appear to contribute to the respective orientation of β-strand I (1–3) and of the extended fragment (4–7) with respect to the rest of the motif. The second group of side chains is composed by His$_{21}$ and Thr$_{23}$ in loop II, by Leu$_{20}$ and Cys$_{17}$ in the helix, and by Cys$_{35}$ in β-strand III. These residues likely play a role on the structural organization of loop II. The His$_{21}$ and Thr$_{23}$ side chains are in fact pointing toward the interior of the loop and present many nonbonded contacts with Leu$_{20}$, Cys$_{17}$, and Cys$_{35}$, while the other residues of the loop (Asn$_{22}$ and Ser$_{24}$) point outside, as shown by the values of surface accessibility.

Comparison of five different toxins acting on K$^+$ channels (Table III) shows that three cases have to be distinguished. Chtx, Chtx-2, and iberiotoxin have similar characteristics. Most of the residues of the hydrophobic cluster are conserved, with the replacement of Val$_5$ by Glu and of Val$_{16}$ by Ile in Chtx-2. These replacements may be consistent with the conservation of a hydrophobic cluster; the Glu side chain possesses indeed two hydrophobic methylene groups. Furthermore, the short loop II has the same length in these three toxins with an aromatic side chain (His or Phe) at position 21 (using the numbering of Chtx) and a Thr or Val (which are isosteric) at position 23. The hydrophobic cluster may be conserved in noxiustoxin too, the greater difference being the substitution of Val$_{16}$ by Pro, but loop II is longer in noxiustoxin than in Chtx and has likely a different structure. Finally, scyllatoxin is very different from the other toxins. The β-strand I is missing, and the connection between the helix and the β-strand II is shorter than in charybdotoxin. The only conserved residue between scyllatoxin and the others is Leu$_{20}$. It is worth noting that the five residues forming the hydrophobic

Table III: Comparison of Short-Chain Scorpion Toxins Acting on K+ Channels[a]

		b b b e e e a a a a a a a a a a b b b b b b b b
Lqh	Chtx	Z F T N V S C T T S ***K*** ***E*** C W S V C Q ***R*** L - **H** N **T** S ***R*** G ***K*** C M N ***K*** ***K*** C ***R*** C ***Y*** S
Lqh	Chtx-2	Z F T Q ***E*** S C T A S N Q C W S I C ***K*** ***R*** L - **H** N **T** N ***R*** G ***K*** C M N ***K*** ***K*** C ***R*** C ***Y*** S
Bt	Iberiotoxin	Z F T D V D C S V S ***K*** ***E*** C W S V C ***K*** ***R*** L - F G V D ***R*** G ***K*** C M G ***K*** ***K*** C ***R*** C ***Y*** Q
Cn	Noxiustoxin	T I I N V K C T S P ***K*** Q C S K P C K E L Y G S S A G A ***K*** C M N G ***K*** C K C ***Y*** N N
		a a a a a a a a a a b b b b b b b b b b
Lqh	Scyllatoxin	F A C N - L R M C Q L S C R S L G - - - L L G ***K*** C I G D ***K*** C E C V K H

[a] The sequences of five toxins have been aligned with respect to the conserved positions of the six half-cystines. Charybdotoxin (Chtx), charybdotoxin-2 (Chtx-2), and scyllatoxin were isolated from the venom of *Leirus quinquestriatus hebraeeus* (Lqh), noxiustoxin was isolated from the venom of *Centruroides noxius* Hoffman (Cn), and iberiotoxin was isolated from the venom of *Buthus tamulus* (Bt) (Strong, 1990; Sugg et al., 1990). The disulfide bridges and the secondary structure elements are shown above the sequences: (a) indicates residues in the helix, (b) residues in the β-sheet, and (e) residues in the extended fragment. The conserved residues discussed in the text are outlined. The two residues (H_{21} and T_{23}) of the small loop are in bold type. The charged residues and Tyr_{36} are in bold italic type. The residues of the hydrophobic cluster are in bold bordered type. Z is the one-letter code for pyroglutamic acid.

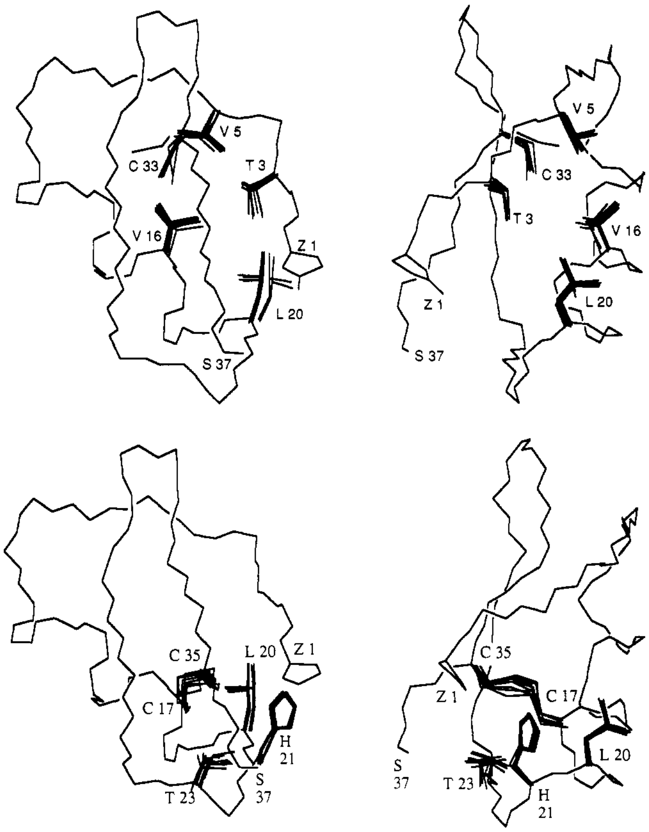

FIGURE 7: Side chains belonging to the first (top) and second (bottom) groups of residues (see text) presented in two different views. The side chains of eight structures have been superimposed. Only one backbone has been represented for clarity. Z is the one-letter code for pyroglutamic acid.

cluster are conserved in the four toxins (i.e., Chtx, Chtx2, iberiotoxin, noxiustoxin) which possess the β-strand I (residues 1–3), while three residues of the cluster (i.e., Thr_3, Val_5, and Val_{16}) are absent in scyllatoxin, which lacks the β-strand I. Much in the same way, the conservation of residues with similar properties at positions 21 and 23 correlates with the conservation of the length of loop II. These observations support our conclusions concerning the structural role of these residues.

Another relevant consequence of charybdotoxin structure is the spatial distribution of the different charged side chains. The toxin contains eight positively charged residues (Lys_{11}, His_{21}, Arg_{19}, Lys_{27}, Lys_{31}, Lys_{32}, Arg_{25}, and Arg_{34}) and two negatively charged residues (Glu_{12} and the C-terminus). Six of these residues, i.e., Arg_{25}, Lsy_{27}, Lys_{31}, Lys_{32}, Arg_{34}, and the terminal carboxylate, are in the β-sheet and the β-turn. Three others (Lys_{11}, Glu_{12}, and Arg_{19}) are located at both ends of the helix. The last (His_{21}) is in the loop connecting the helix to the sheet. This organization results in the formation of two charged surfaces (Figure 8). One of these is located on the helix and presents one negative and two positive charges. The second, located on the β-sheet, is composed of the C-terminal negative charge and of five positive charges.

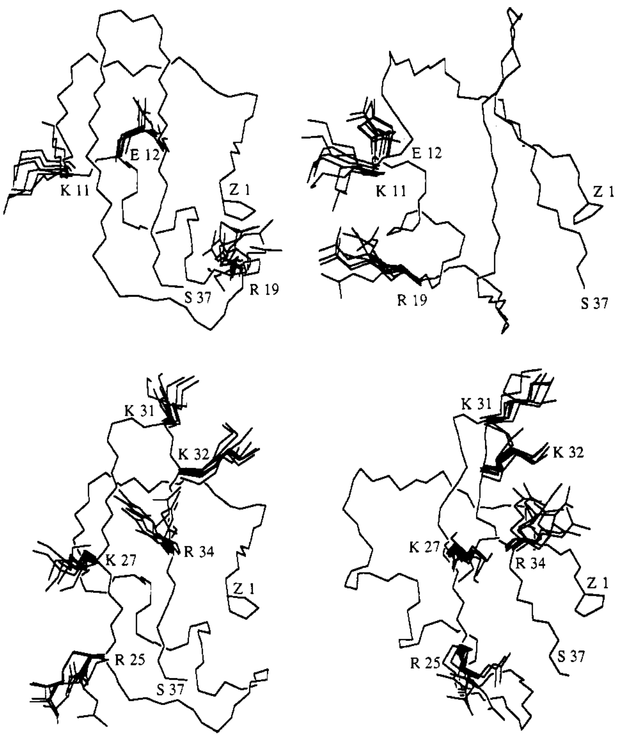

FIGURE 8: Charged residues in the helix (top) and in the β-sheet (bottom) together with the Tyr_{36} presented in two different views. The side chains of eight structures have been superimposed. Only one backbone has been represented for clarity. Z is the one-letter code for pyroglutamic acid.

The side chains forming these two surfaces present several interesting features. In the helix, the side chains of Lys_{11} and Arg_{19} are pointing in the same direction (they are separated by exactly two helix turns). They are both flexible (large ⟨rmsd⟩ values) and exposed to the solvent. The Glu_{12} is more buried. On the β-sheet, Arg_{25}, Lys_{27}, Lys_{31}, and Lys_{32} globally appear to stick in the aqueous phase while Arg_{34} shows a lower surface accessibility (ca. 0.3). In fact, the side chain of Arg$_{34}$ is surrounded by the side chains of Phe$_{2}$, Lys$_{27}$, and Tyr$_{36}$ with which it is involved in a series of short contacts (cf. Results). The contacts, however, seem to correspond to relatively weak interactions; all these side chains are indeed rather flexible (large ⟨rmsd⟩ values). The best defined residue is Lys$_{32}$: the –$C^{\beta}H_2$–$C^{\gamma}H_2$– moiety of Lys$_{32}$ is in close contact with the backbone proton of Val$_{5}$ and Ser$_{6}$ (Figure 1), whereas the remaining part of the side chain is free and accessible to the solvent.

Strikingly, the above mentioned distinction among the five scorpion toxins is also found when the arrangement of the positive side chains are analyzed. The only difference between Chtx, Chtx-2, and iberiotoxin is in the mutation of Lys$_{11}$ to Asn and the presence of an additional Lys at position 18 in Chtx-2. It is concluded that the charged surface on the helix is slightly modified, while the charged surface on the β-sheet is likely conserved. In noxiustoxin, both surfaces are pertubed: the helix presents three positive charges (Lys$_{11}$, Lys$_{15}$, Lys$_{18}$) and one negative charge (Glu$_{19}$), while Arg$_{25}$ and Arg$_{34}$ are substituted by a Gly and a Lys, respectively. Finally, scyllatoxin possesses as does Chtx two positive charges on the helix (Arg$_{11}$ and Arg$_{18}$ instead of Lys$_{11}$ and Arg$_{19}$) but presents a very different β-sheet surface; Arg$_{25}$, Lsy$_{31}$, Arg$_{34}$, and Tyr$_{36}$ are indeed substituted by Leu, Asn, Glu, and Val respectively, and a Lys residue and a His residue are present at the C-terminus of the toxin (positions 37 and 38).

All these observations provide a good basis for analyzing at a molecular level the factors that possibly influence the interaction of Chtx with K^{+} channels. This toxin blocks large-conductance K/Ca^{2+}-dependent channels ($K_{(\mathrm{Ca})}$) and also several classes of other K^{+} channels (Dreyer, 1990).

Previous investigations have indicated that charybdotoxin interacts near the mouth of K^{+} channels (Anderson et al., 1988). This interaction involves both negative charges on the channels, as demonstrated by mutation of the A-type K^{+} channel coded by the *Shaker* gene of *Drosophila melanogaster* (MacKinnon & Miller, 1989; MacKinnon et al., 1989), and positive charges in the C-terminal half of the toxin (Sugg et al., 1990). It has also been reported that iodination of Tyr$_{36}$ (also in the C-terminal part of the molecule) lowers considerably the affinity of Chtx toward $K_{(\mathrm{Ca})}$ channels isolated from rat muscle (Lucchesi et al., 1989). Furthermore, the work of Park and Miller (1992) shows that mutation of the charged residues by Gln has a large influence for Arg$_{25}$, Lys$_{27}$, and Arg$_{34}$ (it accelerates the rate of dissociation from rat muscle $K_{(\mathrm{Ca})}$ channels) and a negligible influence for the other charged residues. Interestingly, the side chains of Arg$_{25}$, Lys$_{27}$, and Arg$_{34}$ are at the surface of the β-sheet, close in space to each other and to Tyr$_{36}$ (Figure 8). They form together with those of Lys$_{31}$ and Lys$_{32}$ a positively charged surface on the sheet. Furthermore, these side chains are rather flexible and are generally exposed to solvent: their mutation is not expected to influence the 3D structure. Altogether, these results hint at the functional importance of Arg$_{25}$, Lys$_{27}$, and Arg$_{34}$ in this part of the molecule. On the other hand, the charged residues of the helix side of the toxin seem to play no direct role on the activity of the toxin. The situation is rather different for scyllatoxin (Auguste et al., 1992), which blocks a different class of K^{+}/Ca^{2+}-dependent channels (small-conductance channels). Chemical modifications of Arg$_{11}$, Arg$_{18}$, and His$_{38}$ (with the numbering of charybdotoxin) abolished both the binding on rat brain $K_{(\mathrm{Ca})}$ channels and the toxin capacity to contract guinea pig tænia coli, while simultaneous modification of Lsy$_{27}$, Lys$_{32}$, and Lys$_{36}$ modifies the activity of the toxin on tænia coil but does not alter the binding on rat brain channels. From this, Auguste et al. conclude that scyllatoxin interacts with its receptor by the helix side of the toxin and that the β-sheet charged surface is important for a second step following toxin binding.

All these observations lead to the conclusion that charybdotoxin and scyllatoxin, although they are organized around the same structural motif, present different structural and functional characteristics. Charybdotoxin possesses the complete motif common to all scorpion toxins, this motif being stabilized in particular by a cluster of hydrophobic side chains. Chtx interacts with its receptor (large conductance K^{+}/Ca^{2+}-dependent channels) by the β-sheet surface. Scyllatoxin is shorter; the β-strand I (residues 1–3) is lacking, and the connection between the helix and the sheet is different from that of charybdotoxin. Scyllatoxin interacts with its receptor (small-conductance K^{+}/Ca^{2+}-dependent channels) by the helix side, but one (or several) lysine residue(s) on the β-sheet is (are) also important for the activity. Another interesting observation is that two residues, Lys$_{27}$ and Lys$_{32}$, are conserved in all these toxins. The effect of Lys to Gln mutation on the activity shows that Lys$_{27}$ is functionally important in charybdotoxin (Park & Miller, 1992). The same conclusion might be true for scyllatoxin. On the other hand, Lys$_{32}$ seems to have no functional role, as no change in the binding is observed in the Lys$_{32}$ → Gln mutant (Park & Miller, 1992). In charybdotoxin, the Lys$_{32}$ side chain (–$C^{\beta}H_2$–$C^{\gamma}H_2$–) presents as mentioned above several nonbonded contacts with the backbone (residues 5–6). Since the Gln residue is likely to interact as Lys$_{32}$ with $C^{\beta}H_2$–$C^{\gamma}H_2$, it may be suggested that Lys$_{32}$ in charybdotoxin has possibly a structural role.

ACKNOWLEDGMENT

We are grateful to Dr. Chul-Seung Park and Dr. Christopher Miller for providing the results of their experiments prior to publication. We thank Drs. Vincent Dive and Claudio Vita (DIEP, Saclay) for numberous fruitful discussions. We acknowledge Prof. K. Wüthrich for providing us a copy of the program DIANA.

REFERENCES

Anderson, C., MacKinnon R., Smith, C., & Miller, C. (1988) *J. Gen. Physiol. 91*, 317–333.

Aue, W. P., Bartholdi, E., & Ernst, R. R. (1976) *J. Chem. Phys. 64*, 2229–2246.

Auguste, P., Hugues, M., Mourre, C., Moinier, C., Tartar, A., & Lazdunski, M. (1992) *Biochemistry 31*, 648–654.

Bontems, F., Roumestand, C., Boyot, P., Gilquin, B., Doljansky, Y., Ménez, A., & Toma, F. (1991a) *Eur. J. Biochem. 196*, 19–28.

Bontems, F., Roumestand, C., Gilquin, B., Ménez, A., & Toma, F. (1991b) *Science 254*, 1521–1523.

Brünger, A. T. (1988) *X-PLOR manual*, The Howard Hughes Medical Institute and Department of Molecular Biophysics and Biochemistry, Yale University, New Haven, CT.

Brünger, A. T., & Karplus, M. (1991) *Acc. Chem. Res. 24*, 54–61.

Brünger, A. T., Kuriyan, K., & Karplus, M. (1987) *Science 235*, 458–460.

Davis, D. G., & Bax, A. (1985) *J. Am. Chem. Soc. 107*, 2820–2821.

Dreyer, F. (1990) *Rev. Physiol. Biochem. Pharmacol. 115*, 93–136.

Endo, T., & Tamiya, N. (1991) Snake Toxins, in *International Encyclopedia of Pharmacology & Therapeutics* (Harvey, A. L., Ed.) Sect. 134, pp 165–222, Pergamon Press, New York.

Gippert, G. P., Yip, P. F., Wright, P. E., & Case, D. A. (1990) *Biochem. Pharmacol. 40*, 15–22.

Günter, P., Braun, W., & Wüthrich, K. (1991) *J. Mol. Biol. 217*, 517–530.

Kumar, A., Ernst, R. R., & Wüthrich, K. (1980) *Biochem. Biophys. Res. Commun. 95*, 1–6.

Lucchesi, K., Ravindran, A., Young, H., & Moczydlowski, E. (1989) *J. Membr. Biol. 109*, 269–281.

MacKinnon, R., & Miller, C. (1989) *Science 245*, 1382–1385.

MacKinnon, R., Latorre, R., & Miller, C. (1989) *Biochemistry 28*, 8092–8099.

Macura, S., Huang, Y., Suter, D., & Ernst, R. R. (1981) *J. Magn. Reson. 43*, 259–281.

Miller, S., Janin, J., Lesk, A. M., & Chothia, C. (1987) *J. Mol. Biol. 196*, 641–656.

Nilges, M., Clore, G. M., & Gronenborn, A. M. (1988) *FEBS Lett. 229*, 317–324.

Norton, R. S. (1991) *Toxicon 29*, 1051–1084.

Olivera, B. M., Rivier, J., Clark, C., Ramillo, C. A., Corpuz, G. P., Abogadie, F. C., Mena, E. E., Woodward, S. R., Hillyard, D. R., & Cruz, L. J. (1990) *Science 249*, 257–263.

Park, C.-S., & Miller, C. (1992) *Biochemistry* (preceding paper in this issue).

Rance, M., Sørensen, O., Bodenhausen, G., Wagner, G., Ernst, R. R., & Wüthrich, K. (1983) *Biochem. Biophys. Res. Commun. 117*, 479–485.

Redfield, A. G., & Kunz, S. D. (1975) *J. Magn. Reson. 19*, 250–254.

Simard, J. M., & Watt, D. D. (1990) *The Biology of Scorpion* (Polis, G. A., Ed.) pp 415–444, Stanford University Press, Stanford, CA.

Srinivasan, N., Sowdhamini, R., Ramakrishnan, C., & Balaram, P. (1990) *Int. J. Pept. Protein Res. 36*, 147–155.

Strong, P. N. (1990) *Pharmacol. Ther. 46*, 137–162.

Sugg, E. E., Garcia, M. L., Johnson, B. A., Kaczorowski, G. J., Patchett, A. A., & Reuben, J. P. (1990) *Peptides: Chemistry, Structure and Biology* (Rivier, J. E., & Marshall, G. R., Eds.) pp 1069–1070, ESCOM, Leiden, The Netherlands.